

Triplex Glass Laminates with Silicon Quantum Dots for Luminescent Solar Concentrators

Jing Huang, Jingjian Zhou, Tommy Haraldsson, Alden Clemments, Minoru Fujii, Hiroshi Sugimoto, Bo Xu, and Ilya Sychugov*

Luminescent solar concentrator (LSC) is a promising technology to integrate semitransparent photovoltaic (PV) systems into modern buildings and vehicles. Silicon quantum dots (QDs) are good candidates as fluorophores in LSCs, due to the absence of overlap between absorption and emission spectra, high photoluminescence quantum yield (PLQY), good stability, nontoxicity, and element abundance. Herein, LSCs based on Si QDs/polymer nanocomposites are fabricated in a triplex glass configuration. A special polymer matrix (off-stoichiometric thiol-ene, OSTE) is used, which improves Si nanocrystal quantum yield. Herein, a comprehensive investigation to improve the performance of LSCs by exploring different strategies under the guidance of a theoretical description is conducted. Among these strategies, the systematical enhancement of PLQY of the nanocomposite is achieved by tuning the thiol/allyl group ratio in the OSTE matrix. In addition, ligand selection and loading optimization for QDs reduce the total scattering loss in the device. Finally, an optical power efficiency of 7.9% is achieved for an optimized LSC prototype ($9 \times 9 \times 0.6 \text{ cm}^3$, transmittance $\approx 62\%$ at 500 nm) based on Si QDs/OSTE nanocomposite, which shows good potential of this material system in LSC fabrication.

1. Introduction

Building-integrated photovoltaics (BIPVs) is a promising solution to the growing demand for energy and space in urban cities with expanding populations. Luminescent solar concentrators (LSCs), for example, can be integrated into buildings as semitransparent windows with a large surface area and show great potential in improving solar energy harvesting for modern buildings.^[1] A typical LSC consists of a glassy or polymeric optical waveguide embedded with fluorophores, which absorb direct and diffused sunlight and re-emit at longer wavelengths. Most of the emitted light is trapped inside the waveguide and propagates to the edges of the device by total internal reflection (TIR), which is then collected by the attached photovoltaic (PV) cells and converted to electricity. Compared with the surface area that is exposed to sunlight, the edge area of an LSC is much smaller, and therefore,

the emitted light is concentrated at the edges and more intensive radiation flux is guided to PV cells. As a result, photocurrent from the cells can be boosted.^[2]


Despite the great potential of LSCs, they have not yet been extensively commercialized, primarily due to their modest efficiency for large devices. The record power conversion efficiency for an LSC coupled with PV cells is 7.1%,^[3] which is based on organic dyes. However, this value is only valid for a small device ($5 \times 5 \times 0.5 \text{ cm}^3$), and efficiency of an LSC is highly dependent on dimensions of the LSC.^[2a,4] In addition to well-known photostability issues, one limitation of large-area LSCs based on organic dyes is a serious reabsorption loss, arising from a large spectral overlap between their absorption and emission.^[5] To suppress reabsorption losses in LSCs, colloidal quantum dots (QDs), especially low-toxic QDs, can be attractive materials as fluorophores. This is due to their broadband absorption and unique size/composition-dependent optical properties, such as structure-engineered Stokes shift, a high photoluminescence quantum yield (PLQY), and desirable photo/chemical stability.^[6] Recently, a CuInS_2 QD-based LSC with dimensions of $30 \times 30 \times 0.7 \text{ cm}^3$ has achieved an optical efficiency of 6.8% (400–750 nm transmittance around 40%), which is promising for the large-scale application of LSCs.^[7] In addition, LSCs based on silicon QDs have drawn increasing interest in recent years.^[8]

Dr. J. Huang, J. Zhou, Dr. A. Clemments, Prof. I. Sychugov
 Department of Applied Physics
 KTH – Royal Institute of Technology
 16440 Stockholm, Sweden
 E-mail: ilyas@kth.se

Dr. T. Haraldsson
 Department of Micro and Nanosystems
 KTH – Royal Institute of Technology
 10044 Stockholm, Sweden

Prof. M. Fujii, Prof. H. Sugimoto
 Department of Electrical and Electronic Engineering
 Kobe University
 Rokkodai, Nada, Kobe 657-8501, Japan

Dr. B. Xu
 Department of Chemistry
 KTH – Royal Institute of Technology
 10044 Stockholm, Sweden

 The ORCID identification number(s) for the author(s) of this article can be found under <https://doi.org/10.1002/solr.202000195>.

© 2020 The Authors. Published by WILEY-VCH Verlag GmbH & Co. KGaA, Weinheim. This is an open access article under the terms of the Creative Commons Attribution License, which permits use, distribution and reproduction in any medium, provided the original work is properly cited.

DOI: 10.1002/solr.202000195

Due to nontoxicity, widespread element abundance, tunable photoluminescence properties, and rich surface functionality, Si QDs are considered as interesting alternatives to QDs which contain low-abundance elements, such as indium. Furthermore, the indirect bandgap nature of Si QDs^[9] promises a large Stokes shift between their absorption and emission spectra, and consequently, the reabsorption loss of LSCs based on Si QDs could be almost negligible.^[8e]

Si QD-based LSCs were first demonstrated by embedding Si QDs in a poly(lauryl methacrylate) (PLMA) matrix, with a promising optical power efficiency of 2.85% (dimensions of $12 \times 12 \times 0.26 \text{ cm}^3$, transmittance of 75% across the visible spectrum).^[8e] Thereafter, several attempts have been made to improve optical properties of Si QDs/polymer nanocomposites. The PLQY of the nanocomposite was enhanced up to 60–70% by incorporating Si QDs in the off-stoichiometric thiol-ene (OSTE) matrix. This enhancement in PLQY is unusual for fabricating QD/polymer nanocomposites as the fluorescence of QDs is often quenched during the polymerization process.^[8a] Simultaneously, it has been found that the ester-functionalized Si QDs exhibited good dispersion in poly(methyl methacrylate) (PMMA), significantly reducing the scattering loss in a Si QDs/PMMA matrix.^[8b,8c] Organic chromophores were also covalently attached to the surface of Si QDs to enhance the light harvesting of LSCs, though the PLQY of Si QDs dropped upon covalent functionalization.^[8d] Despite these recent advancements, much work remains to realize the true potential of Si QD-based LSCs. In addition, no work has been reported to use the Si QDs/polymer nanocomposite as an interlayer for laminated glass. This is an alternative structure for LSCs, which replicates some modern windows and features both for the protection of the active layer from the environment and for the enhancement of the unit mechanical strength.^[10] Furthermore, the propagation losses can be reduced by laminating the nanocomposite between two sheets of optically clear glass, due to the shortened optical path within the QD layer.^[6c,11]

In this work, we fabricated LSCs based on Si QDs with the triplex configuration and elucidated relevant loss mechanisms. Our approach was based on the previously developed OSTE polymer matrix, in which the PLQY of Si QDs was reported to be enhanced by surface passivation from the polymerization process.^[8a] The chosen matrix material also possesses some advantageous properties, such as high optical clarity and uniformity, oxygen-scavenging capability, and a fast polymerization rate with low volume shrinkage.^[12] It can also be readily laminated on glass, making the composite suitable for triplex LSC fabrication.^[13] To enhance the performance of LSCs, we conducted a comprehensive study to extract and improve all input parameters, which can influence LSC performance, based on a reported analytic solution.^[4] In particular, the PLQY enhancement of Si QDs when transferred from solution to the QDs/OSTE hybrid solid was systemically investigated, and strategies to improve the PLQY of the nanocomposite was demonstrated. Furthermore, we focused on alleviating scattering losses in the LSC, by carefully choosing capping ligands for Si QDs and optimizing the loading amount of QDs in the nanocomposite. Analysis from the transmission electron microscopy (TEM) images of the microtome-prepared samples revealed that the Si QDs capped by an ester ligand can be dispersed well within

nano- and microclumps in OSTE matrix, resulting in less scattering for the composite. Finally, we fabricated a medium-size ($9 \times 9 \times 0.3 \text{ cm}^3$), highly transparent (transmittance of $\approx 79\%$ at 500 nm) LSC based on the optimized Si QDs/OSTE nanocomposite, with an optical power efficiency of 3.7%, as well as a thicker one ($9 \times 9 \times 0.6 \text{ cm}^3$, transmittance of $\approx 62\%$ at 500 nm), featuring an efficiency of 7.9%. These values put Si QDs on par with other colloidal QDs, such as CuInS₂,^[6c] highlighting potential of this material system, where element abundance and nontoxicity are clear advantages.

2. Results and Discussion

2.1. Synthesis of Si QDs and Fabrication of LSCs

Si QDs were synthesized from a commercial precursor, hydrogen silsequioxane (HSQ), by following a reported method.^[14] Generally, HSQ was thermally decomposed in a reducing atmosphere to yield Si nanocrystals encapsulated in a SiO₂ matrix. Then the annealed HSQ was etched by the HF solution to release Si QDs from the matrix. Nanoparticle size can be tuned by the annealing temperature; thus, the QDs can exhibit fluorescence in different wavelengths.^[14b] In this work, our target wavelength was around 850 nm, where the coupled Si solar cells show a high quantum efficiency (up to 90%). Therefore, 1200 °C was chosen to anneal the HSQ. After HF etching, the obtained hydride-terminated Si QDs were transferred to an argon-filled Schlenk line and then functionalized by methyl 10-undecenoate, for fabricating ester-capped QDs. The TEM image of the as-synthesized Si QDs (Figure S2, Supporting Information) revealed an average particle size of 5–7 nm, which is consistent with other works.^[8a,15] Due to the indirect band-gap nature of Si QDs, a large Stokes shift was observed (Figure S3, Supporting Information), which fulfils the fundamental requirement of fluorophores in LSCs. To fabricate the LSCs based on Si QDs/OSTE nanocomposite, the purified Si QDs were thoroughly mixed with thiol and allyl monomers, as well as a photoinitiator, to form a stable and transparent solution, which was then slowly poured in between two glass sheets. Polymerization was initiated by UV irradiation to prepare triplex glass units.

2.2. Analytical Description for LSCs

The operating principle of an LSC is based on the TIR of emission light from the fluorophore, which is then guided to the edges of the slab and converted to electricity by the attached solar cells. During the propagation of the luminescent light, however, the light could be lost due to several processes, such as emission to the escape cone, reabsorption by the fluorophores, absorption by the matrix, and scattering by defects (inhomogeneity of the polymer and QD agglomerates).^[16] Taking into account all these potential losses, our group has derived an analytical solution to estimate the performance of LSCs with different compositions and designs.^[4] The optical output power of an LSC can be represented as (reflectance neglected)

$$P_{\text{opt}} = \frac{\Phi \cdot a^2 \cdot (1 - T) \cdot \delta \cdot QY \cdot \eta \cdot x \cdot f(x)}{x - \delta \cdot (\alpha_{\text{sc}} + QY \cdot \alpha_{\text{re}})(1 - f(x))} \quad (1)$$

where the waveguiding efficiency function $f(x)$ ($x = \alpha_{sc} + \alpha_{re} + \alpha$) for square geometry is

$$f(x) = \frac{2(2axk - (ka\sqrt{2}x + 1) \cdot e^{-ka\sqrt{2}x} + 2e^{-kax} - 1)}{x^2 a^2 \pi k^2} - \frac{4}{a\pi k} \int_{ka}^{ka\sqrt{2}} \frac{\sqrt{l^2 - (ka)^2}}{l} e^{-xl} dl \quad (2)$$

With Equation (1) and (2), one can quickly predict the optical power output P_{opt} [W] of the device by just putting in values of incoming energy flux Φ [W cm^{-2}], geometry of the slab (side length a [cm] for a square), transmittance of incoming sunlight T , fraction of the emission to the waveguiding mode δ ($\delta = 0.75$ for $n = 1.5$), quantum yield QY of the fluorophores, energy conversion coefficient η of the luminescence ($\eta = 0.6$ for Si QDs, defined as the ratio of photoluminescence and solar peak energies, $\eta = \epsilon_{PL}/\epsilon_{sun}$, where $\epsilon_{PL} \approx 1.5$ eV and $\epsilon_{sun} \approx 2.5$ eV), and scattering coefficient α_{sc} [cm^{-1}], reabsorption coefficient α_{re} [cm^{-1}], and absorption coefficient α [cm^{-1}] of the matrix. Finally, k is a coefficient reflecting 3D geometry: $k \approx 1.14$ for $n = 1.5$. Some variables in Equation (1) generally depend on the wavelength. However, average values can be used for optical power estimates without introducing large errors in most cases. Considering the optimization of LSC performance, δ , k , and η can be treated as constants if certain types of fluorophores and polymers are chosen. In the following parts, we will discuss the influence of the remaining parameters on the performance of the LSC and explore corresponding strategies to improve performance of the LSC based on Si QDs.

2.3. Reabsorption Loss, α_{re}

To minimize the reabsorption loss in the LSC, a large Stokes shift between absorption and emission spectra is necessary for the fluorophore. As shown in Figure S3, Supporting Information, the Stokes shift of our as-synthesized Si QDs was around 400 nm. More specifically, absorption cross section at 850 nm of Si QDs with a size of ≈ 5 nm is around $2 \times 10^{-18} \text{ cm}^2$,^[17] which means that the reabsorption coefficient at 850 nm of an LSC with the Si QD loading of 0.1 wt% (particle concentration of 5.6 μM) is only 0.007 cm^{-1} . This is essentially negligible when the surface area of the device is smaller than 1 m^2 . Therefore, using Si QDs as fluorophores in LSCs can almost completely suppress reabsorption in the device.

2.4. Matrix Absorption Loss, α

Matrix absorption could induce profound influence in LSCs, as shown in Figure S5A, Supporting Information, and becomes pronounced especially for large-sized devices. Though normal soda lime glass is considered as transparent glass, the absorption from the UV to NIR region is usually high (with an absorption coefficient of around 0.5 cm^{-1} at 850 nm),^[18] due to the high content level of iron. Therefore, low-iron or noniron glass is necessary for efficient LSCs. Herein, the absorption of low-iron soda lime glass (Optiwhite, Pilkington) and borosilicate glass (Borofloat, Schott) was evaluated (Figure S5B, Supporting

Information). The absorption coefficients for both of them are much lower than normal soda lime glass, namely 0.07 and 0.03 cm^{-1} , for the low-iron soda lime glass and the borosilicate glass, respectively. In addition, the measured absorption coefficient at 850 nm of our OSTE ($\approx 0.04 \text{ cm}^{-1}$) is comparable to the most used PMMA (0.03 cm^{-1}),^[19] which implies that OSTE could also be a suitable host polymer matrix for fluorophores in LSCs in the aspect of low matrix absorption. To further decrease the matrix absorption, N-BK7 glass and fluorinated PMMA can be used (the absorption coefficient of them are reported to be below 0.001 cm^{-1});^[16b] however, their high cost greatly limits their application for large areas.

2.5. Photoluminescence Quantum Yield

To improve the performance of an LSC, one of the most effective approaches is to enhance the PLQY of fluorophores. Most of the LSCs with decent optical efficiencies are based on QDs with PLQY above 50%.^[6c,6e,6f,20] Surface functionalization of the hydride-terminated Si QDs with organic ligands has made the synthesis of the stable colloidal Si QD solution with PLQY above 50% feasible.^[21] However, to obtain Si QDs/polymer nanocomposite with a high PLQY is still a challenge, as the QDs could be sensitive to a radical attack during polymerization process and subjected to luminescence quenching in the solid matrix.^[22] To the best of our knowledge, most of the nanocomposites based on Si QDs exhibited a PLQY below 50%, or even much lower, which can be of great limitation to the performance of LSCs.

Our previous results revealed that embedding Si QDs in OSTE can enhance their PLQY.^[8a] Herein, we systematically studied the enhancement in PLQY when transferring Si QDs from toluene solution to the OSTE matrix. To understand the origin of this enhancement, electron paramagnetic resonance (EPR) measurements were carried out on Si QDs in toluene and in nanocomposites. As shown in Figure 1B, the paramagnetic defect amount on Si QDs decreased upon transferring QDs from toluene solution to OSTE matrix. Namely those on Si QDs in the nanocomposite constituted only 73% of the ones in the toluene solution, as can be deduced from the EPR signal amplitudes for the T/E ratio of 2/1. Although the EPR can detect only specific kinds of paramagnetic defects,^[24] the decrease in the signal strongly suggests that QD surface dangling bonds combined with matrix radicals to form stable covalent bonds during the polymerization process. As a result, some dark particles were turned into bright ones,^[21b] as shown in Figure 1A, and thereby, the total PLQY of the composite was enhanced. Such a correlation between the PL intensity and the paramagnetic defect density has also been shown in other reports.^[25] Furthermore, we comprehensively investigated the influence of the thiol/allyl group (T/E) ratio to the PLQY enhancement in the nanocomposites, as it was suggested that the passivation probably originates from thiyl radicals.^[8a] Assigning the fraction of persistent “dark” nanocrystals during the polymerization process to D , the relationship between the quantum yield after, QY_2 , and before, QY_1 , the polymerization becomes

$$\text{QY}_2 = 1 - (1 - \text{QY}_1) \times D \quad (3)$$

We extracted D values from previous experiments, where $\text{QY}_{1,2}$ were measured for different T/E ratios.^[8a] Results are

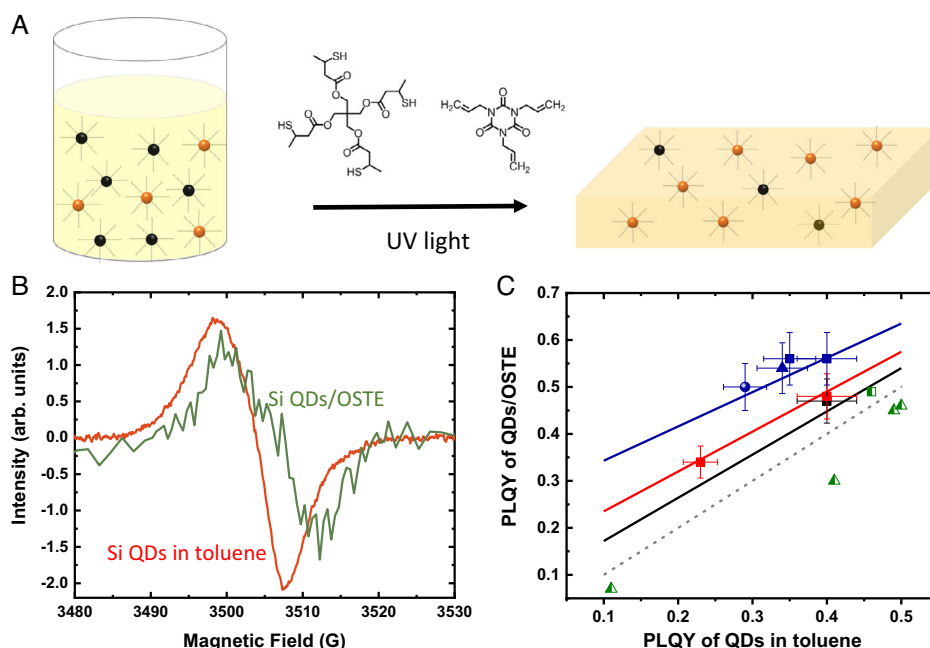


Figure 1. A) Schematic illustration of transferring Si QDs from toluene to OSTE matrix. During polymerization, the dangling bonds on Si QDs are partially passivated by radicals, turning some of the “dark” QDs into “bright” ones. B) The first-derivative EPR spectra of Si QDs in toluene and Si QDs/OSTE nanocomposite (T/E ratio of 2/1). The same amount of QDs was used in the liquid and solid phases. C) PLQY of Si QDs in toluene and for Si QDs/OSTE nanocomposites with different T/E ratios (blue-2/1, red-1.5/1, and black-1/1). Solid lines are from Equation (3); the dotted line refers to unchanged PLQY. Scattered dots are experimental data, and different shapes represent Si QDs capped by different types of ligands: square ester, triangle alkane, and circle acid. The PLQY values of Si QDs in solution and solid from other works (non-OSTE polymer) are also shown as green half-filled dots.^[8c,8e,23]

shown in Table S1, Supporting Information, and the obtained linear dependencies QY_2 (QY_1) for three different D values are shown as solid lines in Figure 1C. The grey dotted line represents no change in PLQY, i.e. $D = 1$. To validate Equation (3), here we carried out QY measurements on nanocomposites fabricated with different T/E ratios, varying surface ligands. The results are shown as the filled dots in Figure 1C and shown in Table S1, Supporting Information. We can see that all the experimental points with all kinds of T/E ratios from this work indeed fall on the lines from Equation (3) within error bars. This result holds regardless of the choice of passivating ligands (esters, alkanes, or acids). Thereby we have confirmed that the PLQY of Si QDs can indeed be enhanced when transferring from solution to OSTE matrix, and the enhancement can be tuned by the T/E ratio in the OSTE matrix. Benefitting from this surface passivation and PLQY enhancement effect, a PLQY above 55% (T/E ratio of 2/1) of the LSC can be reproducibly achieved. Apparently, this enhancement rule does not apply to the nanocomposite of Si QDs with the polymers lacking thiyl radicals, as manifested by the work based on other Si/polymer hybrids (shown by green half-filled dots in Figure 1C).^[8c,8e,23a]

The PLQY dependence on the excitation wavelength of Si QDs/OSTE nanocomposites is presented in Figure S6A, Supporting Information, revealing a uniform response in the range from 400 to 520 nm. The long-term stability under the ambient environment of the corresponding LSC is shown in Figure S6B, Supporting Information, indicating that there is no degradation of the LSC after seven months of storage under

ambient conditions. This result also suggests that OSTE matrix is advantageous compared with the often used PMMA, which may be insufficient for protecting Si QDs from oxidation.^[8c] It was proven separately that OSTE acts as an effective oxygen barrier for the embedded nanoparticles.^[13,26]

2.6. Optical Quality and Scattering Loss, α_{sc}

Scattering loss induced by QD agglomerates can be detrimental both to the perceived optical quality and to the performance of LSC devices. However, incompatibility of the QD surface and polymer matrix can easily result in the agglomeration of QDs. The previous work demonstrated that numerous agglomerates were formed in the dodecene-capped Si QDs/OSTE nanocomposite films, even when the loading of QDs in the film was extremely low (0.01 wt%).^[8a] These agglomerates could be accounted to unmatched polarities of the Si QD surface moieties and OSTE monomers, in which the dielectric constant (ϵ) of dodecane is 2 and that of thiol-ene is around 5.^[27] To increase the compatibility of the QD surface and polymer matrix, we tried both to increase the polarity of the QD surface and to decrease the polymer polarity. For the decreasing polarity of the polymer, a new thiol monomer was introduced, in which there is one more methyl group at the end of each chain (shown in Figure S7, Supporting Information). To increase the polarity of the QD surface, methyl 10-undecenoate and dodecanoic acid, the dielectric constants of whose corresponding moieties after being capped to QDs are 3.7^[28] and 6, respectively, were applied as capping

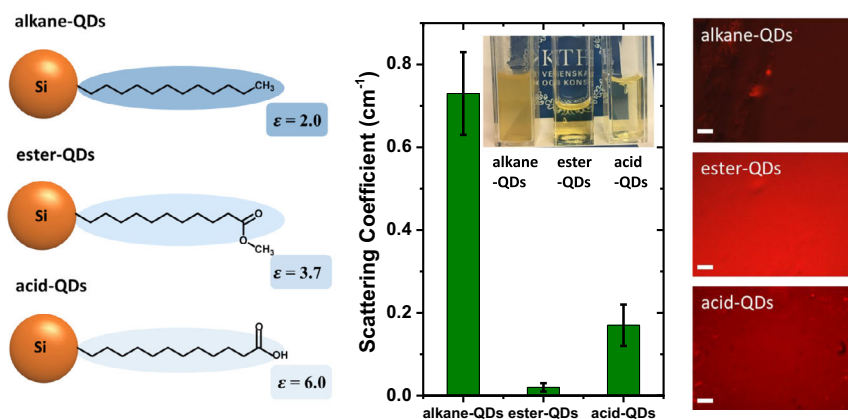


Figure 2. Illustration of Si QDs capped by three kinds of ligands with different dielectric constants (left), and scattering coefficients of Si QDs/OSTE nanocomposites fabricated from these three kinds of ligands, with the corresponding photograph inserted (middle). To the right are real color micro-PL images of Si QDs/OSTE nanocomposites prepared with QDs capped by different kinds of ligands (scale bar is 10 μm).

ligands for Si QDs. The obtained QDs will be referred to as ester QDs and acid QDs, as shown in **Figure 2**, left. As a reference, dodecene was also used as the capping ligand for QDs, and those are referred to as alkane QDs.

Figure 2 (middle) shows the scattering coefficients (at 850 nm) of the nanocomposites fabricated with different ligand-capped Si QDs. They were measured with a “bucket” detector on the samples with the same concentration of Si QDs (0.0125 wt%, detailed in Section S1, Supporting Information). Due to the incompatible polarities of the polymer and the QD surface, the scattering coefficient of the nanocomposite based on alkane QDs is around 0.73 cm^{-1} , corresponding to a completely hazed nanocomposite. The scattering coefficient of the nanocomposite based on acid QDs (0.17 cm^{-1}) is much lower than that of alkane QDs, whereas the scattering coefficient for that based on ester QDs is substantially lower, down to 0.02 cm^{-1} , with a highly transparent appearance. Micro-PL images (Figure 2, right and Figure S8, Supporting Information) also show that no obvious agglomerates at the micrometer scale can be found in the composite based on ester QDs, whereas we can easily find agglomerates in nanocomposites made from alkane and acid QDs.

To further confirm that scattering is suppressed in the ester QD sample, we measured the PLQY of LSC devices ($5.0 \times 1.5 \times 0.1 \text{ cm}^3$) with and without covering the edges. If there is no scattering loss, the fluorescence coming out from the top and bottom surfaces should originate solely from the escape cone, which is $\approx 25\%$ of the total fluorescence for the polymer with a reflective index of ≈ 1.5 . Table S2, Supporting Information, shows results from such PLQY measurements in an integrating sphere. When ester QDs were used to fabricate the LSC device, the emission from the device’s top and bottom surfaces only accounted to $\approx 25\%$ of the total emission, implying that scattering has been suppressed almost completely in this small-area LSC. The PLQY ratios for the devices with alkane QDs (35%) and acid QDs (28%) are both higher than that of ester QDs, consistent with the higher scattering coefficients. Therefore, we conclude that the polarity of ester QDs is more similar with the OSTE matrix used in this work, whereas the polarity of acid QDs might be too high to form a good dispersion

in OSTE. Actually, the ester capped Si QDs can disperse well not only in OSTE, but also in PMMA, as demonstrated by the Minnesota group,^[8b,8c] and the good dispersion should also come from their similar dielectric constants (the dielectric constant of PMMA is also reported to be $3.7^{[29]}$).

In addition to the surface polarity, nanoparticle concentration $N [\text{cm}^{-3}]$ is also a significant factor, affecting scattering in the nanocomposite. Herein, we increased the loading amount of ester Si QDs in the nanocomposite gradually from 0.00625 wt% to 0.1 wt% (corresponding to a particle concentration from 2.1×10^{14} to $3.4 \times 10^{15} \text{ cm}^{-3}$) and measured the corresponding scattering coefficients with the bucket detector. From **Figure 3**, we can see that the scattering coefficient of the composite steadily increases with higher QD loading, and the slope turns out to be ≈ 2 for the fitted line in a log–log scale. Theoretically, in the limit of individual particles, the linear scattering coefficient can be written through the scattering cross-section σ_{sc} as $\alpha_{\text{sc}} = \sigma_{\text{sc}} N$. Practically, however, it may deviate from the linear dependence

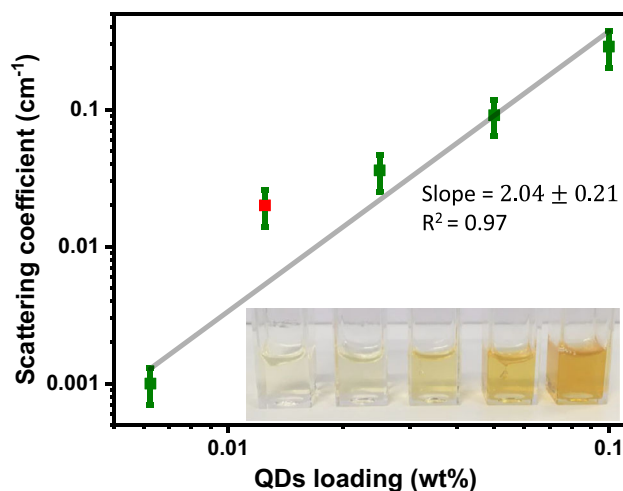


Figure 3. Scattering coefficients of ester Si QDs/OSTE nanocomposites with different loadings; inset is a photograph showing these five nanocomposites under ambient light.

on N due to particle agglomeration, especially at a higher concentration of QDs. Agglomerates with the size smaller than the wavelength can be treated by the Rayleigh theory of scattering. Their scattering cross-section σ_{sc} is very sensitive to the agglomerate size, being proportional to the power of six (and inversely to the wavelength to the power of four). Accordingly, the relationship between scattering coefficient α_{sc} and particle concentration N can be expressed by as (see detailed statistical derivation from Poisson distributions in Section S4, Supporting Information; r is an effective interaction radius)

$$\alpha_{sc}(N) = \frac{4}{3}\pi r^3 \sigma_{sc} N^2 \quad (4)$$

So in the case of agglomeration the scattering coefficient is expected to be proportional to the square of concentration, which is in good agreement with the slope of the fitted line in Figure 3.

Accordingly, the QD concentration should be carefully chosen for fabrication of LSCs. On the one hand, the concentration of QDs should be high enough to provide sufficient sunlight absorption and achieve adequate power output. On the other hand, a high QD concentration might substantially increase scattering loss in the waveguide layer, as shown in Figure 3. For example, though the scattering coefficient is only 0.001 cm^{-1} for the nanocomposite with the QD loading of 0.00625 wt%, which can be deemed as agglomeration free, absorption of the resulting device is greatly limited. When the QD loading goes up to 0.1%, the scattering coefficient increases to 0.29 cm^{-1} , which can result in serious scattering losses for large-area devices. If the QD loading is kept at 0.05 wt% or slightly lower, the scattering coefficient of the nanocomposite will be below 0.1 cm^{-1} and moderate absorption could be obtained, which is still applicable for LSCs with a large size.^[8c]

To further investigate the origin of scattering in the nanocomposite, TEM measurements were carried out on nanocomposites based on ester QDs with the loading of 0.05 wt%. The composite was sliced with an ultra-microtome to get a thin sample (around 100 nm) for the measurement. In general, the atomic number contrast between Si QDs and a sulfur-containing polymer is expected to be low. From an overview image of the nanocomposite, we found many micro- and nanoclumps in the polymer matrix (Figure 4A). When the clumps were zoomed in (Figure 4B), numerous bright dots showed up. When the magnification was further increased, we can clearly determine the morphology of bright dots, as shown in Figure 4C. Most of the dots were monodispersed in the matrix and sized mainly in 4–7 nm with a faceted appearance, which is consistent with the as-synthesized QD appearance in the same microscope (Figure S2, Supporting Information). As a reference, no such dots could be found in the blank OSTE polymer (Figure 4D). Therefore, we conclude that these bright dots in the TEM images were Si QDs embedded in the OSTE matrix. This unusual appearance in a bright-field TEM image could be attributed to a negative stain effect by the residual organic ligand solution from QDs, which is explained in Section S3, Supporting Information.

So the structural characterization indicates that the Si QDs were dispersed in micro- and nanodroplets, possibly from the residual ligand solution in the polymer matrix. Within the droplets, the Si QDs tended to be separated, whereas some

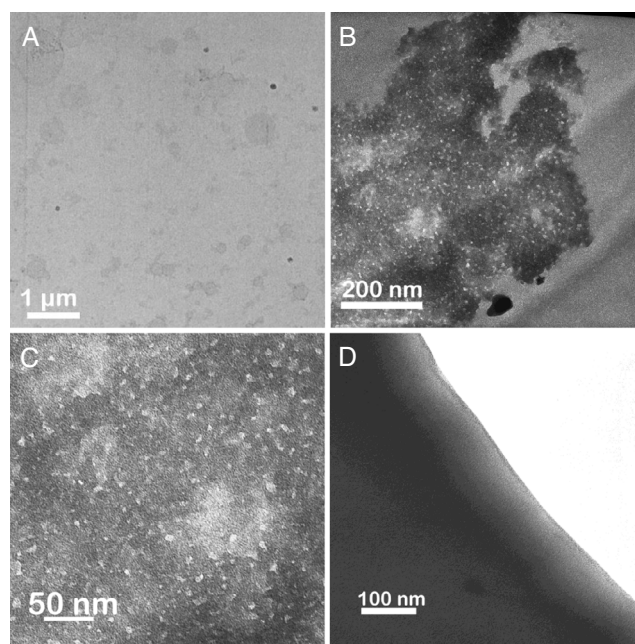


Figure 4. A, B, C) TEM image of Si QDs/OSTE nanocomposites based on ester Si QDs with loading amount of 0.05 wt% at different magnifications. D) TEM image of a blank OSTE polymer (no QDs).

agglomeration statistically occurred within a small interaction radius. Such nonuniformities cannot be resolved in micro-PL images of the sample (Figure S9, Supporting Information), which highlights the importance of the structural imaging of the nanocomposites. Other works on luminescent nanocomposites, with a rare exception,^[30] typically overlook this point. Although the particle load is too low to change the polymer refractive index, micro- and nanoclumps increase the effective concentration of QDs in the nanocomposite. This leads to more statistical agglomeration under the same nominal load of nanoparticles. Therefore, a good dispersion at the microscale is as important as the lack of aggregation at the nanoscale. For a uniform QD distribution the theoretical line in Figure 3 will shift to the right, allowing a higher QD load with a low scattering loss. Thus a practical way to further reduce scattering could be extensive purification of the QD solution before polymerization to avoid such clumps.

2.7. Device Fabrication

Based on the earlier results, Equation (1) and (2) were used to predict the performance of LSC devices using the ester Si QDs with a loading fraction of 0.025, 0.5, and 0.1 wt% (thickness of 3 mm), and the results are shown in Figure 5A. With the increment of QD loading in the nanocomposite, output power of the device also increases, because of stronger sunlight absorption. However, the improvement is sublinear because of stronger scattering and a slight haze indeed can be noticed from the LSC made with 0.1 wt% loading (Figure S10, Supporting Information). Consequently, we chose the QD loading as 0.05 wt% to fabricate an LSC device prototype (active layer size was $9 \times 9 \times 0.3 \text{ cm}^3$).

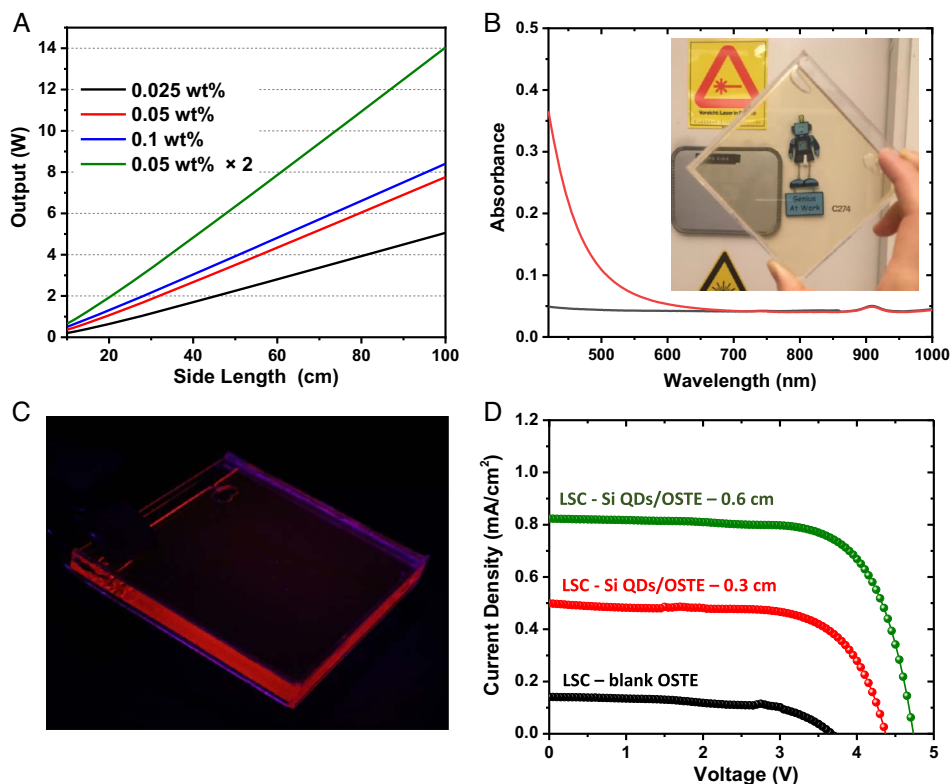


Figure 5. A) Device optical power output calculation results of LSCs with different loadings of ester-capped Si QDs; detailed parameters included in the calculation shown in Table S3, Supporting Information. B) Absorption spectra of the LSCs ($9 \times 9 \times 0.3 \text{ cm}^3$) with (red) and without (black) Si QDs. A photograph of LSC based on Si QDs/OSTE nanocomposites with the ester-capped Si QD loading of 0.05 wt% under ambient light is inserted. The photo was taken when distances between camera and the LSC and the LSC and object were $\approx 0.5 \text{ m}$, to show low haze. C) Photograph of the same LSC under UV irradiation. D) J - V curves of Si solar cells attached to the LSCs ($9 \times 9 \times 0.3 \text{ cm}^3$, red, and $9 \times 9 \times 0.6 \text{ cm}^3$, green) based on the Si QDs/OSTE nanocomposites with a QD loading of 0.05 wt%. A curve measured from the reference LSC ($9 \times 9 \times 0.3 \text{ cm}^3$) without QDs is also shown (black).

For fabricating the LSC, the Si QD/OSTE nanocomposite layer was laminated between two sheets of borosilicate glass, to further reduce the effective scattering coefficient in the whole device (discussed in Section S4, Supporting Information).

The absorption spectra of devices made with blank OSTE matrix and with Si QDs/OSTE nanocomposite are shown in Figure 5B. The LSC with a blank polymer showed little absorbance from visible to NIR region, which can be attributed to the low absorption of the OSTE and the borosilicate glass, as well as reflection at the device surfaces in the spectrophotometer. The small bump at 910 nm can be assigned to the C–H vibration overtone (fourth harmonics) in the polymer matrix. After embedding Si QDs into the OSTE matrix, we can see that the absorbance only increased in the region with wavelengths below 650 nm. No additional absorption in the region of longer wavelength was introduced, which was consistent with absorption of Si QDs in solution. It reveals good optical quality of the devices, as no scattering-related loss appeared. The inserted image in Figure 5B also shows that the device was highly transparent and uniform with an obvious yellow color tint from the absorption of Si QDs. Under UV irradiation (Figure 5C), we can see that the QD fluorescence was effectively guided to the edges and very little portion was emitted from the top and bottom surfaces, which further emphasizes low scattering losses in the device.

To evaluate the performance of the device, a custom-sized Si solar cell was attached to one edge of the LSC by glass glue, and the rest of the edges were uncovered. Then the LSC was placed under a conventional AM 1.5G solar simulator with illumination perpendicular to the surface. No reflector or back diffuser was put beneath the device. J - V measurements were carried out on LSC devices both with and without QDs, with the obtained J - V curves shown in Figure 5D (red curve) and the detailed parameters shown in Table S4, Supporting Information. Under illumination of 0.1 W cm^{-2} , an optical power efficiency η_{opt} (power coming out from LSC edge/power coming in from the top surface) of $\approx 3.7\%$ was obtained for the device ($9 \times 9 \times 0.3 \text{ cm}^3$, detailed calculation is shown in, Section S5, Supporting Information).

Despite the fact that this optical efficiency is comparable with other works on Si QD LSCs with a similar size,^[8e] it still cannot satisfy the requirement of real applications for an LSC, i.e., output $> 50 \text{ W m}^{-1}$ with a visible light transparency $> 50\%$.^[6c] This could be attributed to limited sunlight absorption of QDs in the LSC, as transmittance at 500 nm of this device is as high as 79%. To improve the light absorption of the LSC, a thicker nanocomposite layer could be used as an alternative to raise the QD loading. As shown by the calculation results in Figure 5A, if the thickness of the nanocomposite layer is doubled for the sample

with QD loading of 0.05 wt%, the output of the resultant LSC will be dramatically higher than that of the device with 0.1 wt% for current nanocomposites. Accordingly, an LSC with the size of $9 \times 9 \times 0.6 \text{ cm}^3$ was fabricated. As displayed in Figure S13, Supporting Information, the absorption of the thicker device was higher than that of the original one, and simultaneously, the optical quality of it was as good as the original one. As a result, the performance of the solar cell that was attached on the thicker LSC greatly improved, as shown in Figure 5D (green curve), and the corresponding optical power efficiency was determined to be around 7.9%, with detailed PV parameters and calculations shown in Figure S14 and Table S5, Supporting Information. The PV performance of larger-area devices with an even thicker active layer, and with presumably further suppressed scattering, will be studied in our future work.

3. Conclusion

In summary, triplex-structured LSCs based on Si QDs/OSTE nanocomposites were demonstrated. Our results show that the performance of LSCs based on Si QDs could be improved from several aspects, such as using a triplex configuration for fabricating the devices and choosing optical clear glass as float glass. Numerous measurements have confirmed that PLQY of Si QDs can indeed be enhanced by incorporating them into OSTE matrix, and the enhancement could be tuned by the thiol/allyl group ratio in the polymer. Furthermore, using an ester as a capping ligand for QDs efficiently improved the dispersion of Si QDs in the OSTE matrix, significantly suppressing scattering loss in the nanocomposite. At the same time, QD loading should also be chosen at a moderate level as it can significantly influence both sunlight absorption and scattering in the device. With respect to this point, the analytical formula can be used to predict optical efficiencies of LSCs based on different parameters and give instructions on device optimization. Upon all the discussion and results, a medium-sized LSC ($9 \times 9 \times 0.6 \text{ cm}^3$) was fabricated, with an optical power efficiency of $\approx 7.9\%$, which is comparable with the high-performance LSCs based on other QDs. Thus, we have demonstrated that the performance of Si QDs for LSCs is very similar to the state of the art of their conventional direct bandgap counterparts, rendering attractive further developments in this material system.

Supporting Information

Supporting Information is available from the Wiley Online Library or from the author.

Acknowledgements

This work was supported by Swedish Energy Agency (46360-1). The authors also greatly thank Professor Jan Linnors (KTH) for his valuable discussions on the whole project, Professor Licheng Sun (KTH) for his generous help in I - V measurements of the device, and Professor Geoffrey Daniel (SLU) and Dr. Jie Gao (SLU) for their helpful discussions on the TEM measurements on nanocomposites. H.S. acknowledges the support from JSPS KAKENHI (grant no. 18K14092).

Conflict of Interest

The authors declare no conflict of interest.

Keywords

glass laminates, luminescent solar concentrators, nanocomposites, silicon quantum dots

Received: April 9, 2020

Revised: June 1, 2020

Published online:

- [1] a) W. H. Weber, J. Lambe, *Appl. Opt.* **1976**, *15*, 2299; b) A. Goetzberger, W. Greube, *Appl. Phys.* **1977**, *14*, 123.
- [2] a) V. I. Klimov, T. A. Baker, J. Lim, K. A. Velizhanin, H. McDaniel, *ACS Photonics* **2016**, *3*, 1138; b) M. G. Debijs, P. P. C. Verbunt, *Adv. Energy Mater.* **2012**, *2*, 12.
- [3] L. H. Slooff, E. E. Bende, A. R. Burgers, T. Budel, M. Pravettoni, R. P. Kenny, E. D. Dunlop, A. Büchtemann, *Phys. Status Solidi RRL* **2008**, *2*, 257.
- [4] I. Sychugov, *Optica* **2019**, *6*, 1046.
- [5] a) N. C. Giebink, G. P. Wiederrecht, M. R. Wasielewski, *Nat. Photonics* **2011**, *5*, 694; b) L. Desmet, A. J. M. Ras, D. K. G. de Boer, M. G. Debijs, *Opt. Lett.* **2012**, *37*, 3087.
- [6] a) S. Sadeghi, H. Bahmani Jalali, R. Melikov, B. Ganesh Kumar, M. Mohammadi Aria, C. W. Ow-Yang, S. Nizamoglu, *ACS Appl. Mater. Interfaces* **2018**, *10*, 12975; b) Y. Zhou, H. Zhao, D. Ma, F. Rosei, *Chem. Soc. Rev.* **2018**, *47*, 5866; c) M. R. Bergren, N. S. Makarov, K. Ramasamy, A. Jackson, R. Guglielmetti, H. McDaniel, *ACS Energy Lett.* **2018**, *3*, 520; d) F. Meinardi, H. McDaniel, F. Carulli, A. Colombo, K. A. Velizhanin, N. S. Makarov, R. Simonutti, V. I. Klimov, S. Brovelli, *Nat. Nanotechnol.* **2015**, *10*, 878; e) K. Wu, H. Li, V. I. Klimov, *Nat. Photonics* **2018**, *12*, 105; f) H. Li, K. Wu, J. Lim, H.-J. Song, V. I. Klimov, *Nat. Energy* **2016**, *1*, 16157; g) Y. Zhou, D. Benetti, Z. Fan, H. Zhao, D. Ma, A. O. Govorov, A. Vomiero, F. Rosei, *Adv. Energy Mater.* **2016**, *6*, 1501913.
- [7] A. Anand, M. L. Zaffalon, G. Gariano, A. Camellini, M. Gandini, R. Brescia, C. Capitani, F. Bruni, V. Pinchetti, M. Zavelani-Rossi, F. Meinardi, S. A. Crooker, S. Brovelli, *Adv. Funct. Mater.* **2020**, *30*, 1906629.
- [8] a) A. Marinins, R. Zandi Shafagh, W. van der Wijngaart, T. Haraldsson, J. Linnros, J. G. C. Veinot, S. Popov, I. Sychugov, *ACS Appl. Mater. Interfaces* **2017**, *9*, 30267; b) S. K. E. Hill, R. Connell, J. Held, C. Peterson, L. Francis, M. A. Hillmyer, V. E. Ferry, U. Kortshagen, *ACS Appl. Mater. Interfaces* **2020**, *12*, 4572; c) S. K. E. Hill, R. Connell, C. Peterson, J. Hollinger, M. A. Hillmyer, U. Kortshagen, V. E. Ferry, *ACS Photonics* **2019**, *6*, 170; d) R. Mazza, A. Gradone, S. Angeloni, G. Morselli, P. G. Cozzi, F. Romano, A. Vomiero, P. Ceroni, *ACS Photonics* **2019**, *6*, 2303; e) F. Meinardi, S. Ehrenberg, L. Dharmo, F. Carulli, M. Mauri, F. Bruni, R. Simonutti, U. Kortshagen, S. Brovelli, *Nat. Photonics* **2017**, *11*, 177.
- [9] J.-W. Luo, S.-S. Li, I. Sychugov, F. Pevero, J. Linnros, A. Zunger, *Nat. Nanotechnol.* **2017**, *12*, 930.
- [10] C. W. Miller, J. Shaw, International patent WO 2009/010423 A1, **2009**.
- [11] G. Liu, R. Mazza, Y. Wang, H. Zhao, A. Vomiero, *Nano Energy* **2019**, *60*, 119.
- [12] C. F. Carlborg, T. Haraldsson, K. Öberg, M. Malkoch, W. van der Wijngaart, *Lab on a Chip* **2011**, *11*, 3136.

- [13] C. Resetco, B. Hendriks, N. Badi, F. Du Prez, *Mater. Horiz.* **2017**, *4*, 1041.
- [14] a) C. M. Hessel, E. J. Henderson, J. G. C. Veinot, *Chem. Mater.* **2006**, *18*, 6139; b) R. J. Clark, M. Aghajamali, C. M. Gonzalez, L. Hadidi, M. A. Islam, M. Javadi, M. H. Mobarok, T. K. Purkait, C. J. T. Robidillo, R. Sinelnikov, A. N. Thiessen, J. Washington, H. Yu, J. G. C. Veinot, *Chem. Mater.* **2017**, *29*, 80.
- [15] C. M. Hessel, J. Wei, D. Reid, H. Fujii, M. C. Downer, B. A. Korgel, *J. Phys. Chem. Lett.* **2012**, *3*, 1089.
- [16] a) C. Tummeltshammer, A. Taylor, A. J. Kenyon, I. Papakonstantinou, *Sol. Energy Mater. Sol. Cells* **2016**, *144*, 40; b) F. Meinardi, F. Bruni, S. Brovelli, *Nat. Rev. Mater.* **2017**, *2*, 17072.
- [17] J. Valenta, M. Greben, Z. Remeš, S. Gutsch, D. Hiller, M. Zacharias, *Appl. Phys. Lett.* **2016**, *108*, 023102.
- [18] M. Rubin, *Sol. Energy Mater.* **1985**, *12*, 275.
- [19] N. Ioannides, E. B. Chunga, A. Bachmatiuk, I. G. Gonzalez-Martinez, B. Trzebicka, D. B. Adebimpe, D. Kalymnios, M. H. Rummeli, *Mater. Res. Express* **2014**, *1*, 032002.
- [20] R. Sumner, S. Eiselt, T. B. Kilburn, C. Erickson, B. Carlson, D. R. Gamelin, S. McDowall, D. L. Patrick, *J. Phys. Chem. C* **2017**, *121*, 3252.
- [21] a) M. A. Islam, M. H. Mobarok, R. Sinelnikov, T. K. Purkait, J. G. C. Veinot, *Langmuir* **2017**, *33*, 8766; b) F. Sangghaleh, I. Sychugov, Z. Yang, J. G. C. Veinot, J. Linnros, *ACS Nano* **2015**, *9*, 7097.
- [22] H. Zhang, C. Wang, M. Li, X. Ji, J. Zhang, B. Yang, *Chem. Mater.* **2005**, *17*, 4783.
- [23] a) A. Marinins, Z. Yang, H. Chen, J. Linnros, J. G. C. Veinot, S. Popov, I. Sychugov, *ACS Photonics* **2016**, *3*, 1575; b) D. Chen, W. Sun, C. Qian, A. P. Y. Wong, L. M. Reyes, G. A. Ozin, *Adv. Optical Mater.* **2017**, *5*, 1700237.
- [24] R. N. Pereira, D. J. Rowe, R. J. Anthony, U. Kortshagen, *Phys. Rev. B* **2012**, *86*, 085449.
- [25] a) X. Liu, S. Zhao, W. Gu, Y. Zhang, X. Qiao, Z. Ni, X. Pi, D. Yang, *ACS Appl. Mater. Interfaces* **2018**, *10*, 5959; b) M. Fujii, A. Mimura, S. Hayashi, K. Yamamoto, C. Urakawa, H. Ohta, *J. Appl. Phys.* **2000**, *87*, 1855.
- [26] L. Liu, L. Deng, S. Huang, P. Zhang, J. Linnros, H. Zhong, I. Sychugov, *J. Phys. Chem. Lett.* **2019**, *10*, 864.
- [27] J. M. Ko, Y. H. Kang, C. Lee, S. Y. Cho, *J. Mater. Chem. C* **2013**, *1*, 3091.
- [28] T. H. Gouw, J. C. Vlugter, *J. Am. Oil Chem. Soc.* **1964**, *41*, 675.
- [29] K. Yang, X. Huang, M. Zhu, L. Xie, T. Tanaka, P. Jiang, *ACS Appl. Mater. Interfaces* **2014**, *6*, 1812.
- [30] J. Bomm, A. Büchtemann, A. J. Chatten, R. Bose, D. J. Farrell, N. L. A. Chan, Y. Xiao, L. H. Slooff, T. Meyer, A. Meyer, W. G. J. H. M. van Sark, R. Koole, *Sol. Energy Mater. Sol. Cells* **2011**, *95*, 2087.

Supporting information for

Triplex Glass Laminates with Silicon Quantum Dots for Luminescent Solar Concentrators

Jing Huang^a, Jingjian Zhou^a, Tommy Haraldsson^b, Alden Clemments^a, Minoru Fujii^c, Hiroshi Sugimoto^c, Bo Xu^d and Ilya Sychugov^{*a}

^aDepartment of Applied Physics, KTH - Royal Institute of Technology, 16440 Stockholm, Sweden

^bDepartment of Micro and Nanosystems, KTH - Royal Institute of Technology, 10044 Stockholm, Sweden

^cDepartment of Electrical and Electronic Engineering, Kobe University, Rokkodai, Nada, Kobe, 657-8501, Japan

^dDepartment of Chemistry, KTH - Royal Institute of Technology, 10044 Stockholm, Sweden

Section S1. Experimental Details

Synthesis of Si QDs

Commercial hydrogen silsesquioxane (HSQ) powder from Applied Quantum Materials Inc. (Canada) was annealed at 1200 °C in a 5% H₂ and 95% Ar atmosphere for 1 h, resulting formation of black Si QDs/SiO₂ powder. To efficiently release Si QDs from SiO₂ matrix during etching process, the obtained Si QDs/SiO₂ powder was firstly grinded with a mortar and pestle, followed by shaken in ethanol. For etching away the SiO₂ matrix, 100 mg of the fine Si QDs/SiO₂ powder was mixed with 3 ml of ethanol and 3 ml of DI water subsequently in a polypropylene centrifuge tube under magnetic stirring. A 50% aqueous hydrofluoric acid (HF) solution (3 ml) was then slowly added to the mixture under stirring. *Caution: HF solution is extremely dangerous and specific safety equipment is necessary in operation.* The suspension turned yellow after stirring for 1 h, indicating that the Si QDs were released from SiO₂ matrix. The resulted hydride-terminated nanoparticles were collected by extractions with 10 ml of toluene for three times, followed by centrifuged at 11000 rpm for 20 min. The precipitate was then collected for surface passivation.

For surface passivation, the fresh hydride Si QDs were mixed with 3 mL of functionalization ligand (methyl 10-undecenoate) (Sigma-Aldrich, 96%) and the mixture was sonicated for 5 min to get homogeneous wetting. Then the suspension was loaded in a flask and transferred to an argon-charged Schlenk line. The reaction mixture was kept at 150 °C for 19 h under Ar atmosphere, and the brown suspension changed to a clear orange/brown solution, which was kept directly for further application. To obtain the Si QDs powder, 1.5 mL of hexane was firstly added into 0.5 mL of Si QDs ester solution, and then the suspension was centrifuged at 8000 rpm or 5 min to separate Si QDs from the liquid phase. Finally, the supernatant was discarded, and the resulted Si QDs powder was used for fabricating nanocomposites directly.

Reference dodecene capped Si QDs and dodecanoic acid capped Si QDs were obtained from Applied Quantum Materials Inc. (Canada).

Fabrication of LSCs based on Si QDs-OSTE nanocomposite

The thiol monomers were pentaerythritol tetrakis (3-mercaptopbutylate), and the allyl monomers were triallyl-1,3,5-triazine-2,4,6 (1H,3H,5H)-trione, both of them were from Mercene Labs AB, Sweden, as well as the photoinitiator ((1-Hydroxycyclohexyl phenyl ketone, Irgacure-184). For a standard preparation of the nanocomposite with QDs loading of 0.5% by weight, 2 mg of Si QDs powder was dispersed in 0.96 g of allyl monomers first, giving clear orange solution, and then 3.11 g of thiol monomers (to obtain a thiol/allyl group ratio of 2/1) and 0.04 g of initiator were added to the solution. For samples with other QDs loading, the amount of Si QDs was changed accordingly. Then the mixture was sonicated for 10 min for thorough mixing, and finally placed in an evacuated desiccator to remove air bubbles from the solution. The homogeneous solution was slowly poured into a prepared glass mold and cured by 360 nm light from a UV torch for 30 s to trigger thiol-ene polymerization reaction. To obtain a uniform nanocomposite interlayer, intensity of UV light should be kept below $0.1 \text{ mW}\cdot\text{cm}^{-2}$. The polymerization was completed after storing the sample in dark for 1 h.

For the optical property measurements of the nanocomposites, the mixed QD-monomer solution was placed in a plastic cuvette before cured by UV irradiation.

Structural and standard absorption measurements

Transmission electron microscope (TEM) images of Si QDs and Si QDs/OSTE nanocomposites were obtained from a Philips CM12 TEM (Philips, Eindhoven, the Netherlands) operated at 40-100 kV. Micrographs were taken on Kodak 4489 film (Eastman Kodak Company, Rochester, NY, USA) and digitalized with an Epson Perfection Pro 750 scanner (Epson, Nagoya, Japan). Ultrathin (ca 100 nm) sections of the nanocomposite were cut on a Reichert ultramicrotome using a diamond knife and collected on copper (200 mesh) grids. Fourier-transform infrared (FTIR) spectra of the nanocomposite and the blank OSTE polymer were recorded from a Bruker IFS 66v/S FTIR spectrophotometer, and FTIR spectrum of Si QDs was obtained from ATR mode on a Nicolet IS10 FTIR spectrophotometer, by directly drop-casting Si QDs in toluene solution on a microscope glass slide. UV-vis absorption spectra were collected on Lambda 750 UV-vis spectrophotometer, and Si QDs were measured in toluene solution.

Electron paramagnetic resonance (EPR) measurement

A 200 μL of Si QDs toluene solution with concentration of 5 mg/mL, and a 91.2 mg of Si QDs/OSTE nanocomposite with QD loading of 0.01 wt% was prepared for EPR measurements. These quantities correspond to the same amount of QDs. The measurements were performed on an EPR spectrometer (Bruker-EMX8/2.7), and carried out at 25 K, 4.235 mW microwave power with modulation amplitude of 5 G at 100 kHz modulation frequency.

Optical measurements

Photoluminescence quantum yield (PLQY)

Photoluminescence spectra and absolute PLQY were measured from a home-built integrating sphere setup. A laser-driven xenon plasma white-light source (Energetiq EQ-99) coupled with a tunable monochromator (SP2150i, Princeton Instruments) was used as excitation source, a 6 inch diameter integrating sphere (Labsphere) provides light collection, and the Peltier element

cooled CCD camera (-75°C, Princeton Instruments) is connected to a spectrometer for the signal acquisition. The setup components were connected to the integrating sphere with multimode optical fibers. The system response curve was obtained by using excitation source with a monochromator, where a calibration was performed with an optical power meter (Newport). This procedure was executed for spectrometer grating center wavelengths used in measurements. Spectra of the samples and the reference samples were corrected using system response curve and subtracted from each other. Unless otherwise specified the excitation at 440 nm was employed for all the sample. The absolute quantum yield was then calculated by the ratio of absorbed and emitted photons. The accuracy of the measurement setup (relative error ~ 10%) was confirmed by performing control measurements on another commercial and research-grade QY measurement tools.

Micro-photoluminescence (Micro-PL) of nanocomposites and LSCs

A Zeiss Observer.Z1m inverted microscope with a 100X objective lens was used for taking micro-PL images of the samples. The samples were excited by a 405 nm laser diode in a dark field configuration, and Zeiss AxionCam color camera attached to a microscope port was used for detection. Imaging depth of field of this far-field microscope is ~ 1 μm.

Scattering measurement

Scattering coefficients of the Si QDs-OSTE nanocomposites were obtained from a “bucket” detector, as illustrated in Figure S1.

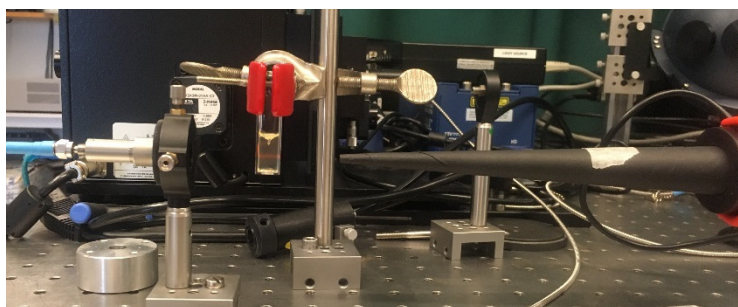


Figure S1. Illustration of scattering measurement with the “bucket” detector.

All the samples were prepared in plastic cuvette (1cm × 1 cm) to reduce surface scattering. Incident light for the measurements was also obtained from a laser-driven xenon plasma white-light source (Energetiq EQ-99) coupled with a tunable monochromator (SP2150i, Princeton Instruments). The incident light at 850 nm was selected for scattering measurement, corresponding to the Si QD luminescence peak position. An optical power meter was used to detect the transmitted light, and a conical screen was connected to the optical power meter to reject all the scattered light and ensure that only transmitted light (ballistic photons) was collected by the optical power meter. The sample with blank OSTE polymer was employed as reference.

If I_0 is the incident light intensity, and I is the detected light intensity by the optical power meter after the sample, then

$$\frac{I}{I_0} = \exp(-(\alpha_{reflection} + \alpha_{OSTE} + \alpha_{abs} + \alpha_{sc}) d)$$

$\alpha_{reflection}$ is the reflection coefficient of the cuvette/air interface [cm^{-1}], α_{OSTE} is the absorption coefficient of OSTE polymer [cm^{-1}], α_{abs} is the absorption coefficient of Si QDs [cm^{-1}], and α_{sc} is the scattering coefficient of the nanocomposite [cm^{-1}]. When only blank OSTE polymer was measured, and the detected light intensity was referred as I_{ref} , then

$$\frac{I_{ref}}{I_0} = \exp(-(\alpha_{reflection} + \alpha_{OSTE}) d),$$

Therefore,

$$\frac{I}{I_{ref}} = \exp(-(\alpha_{abs} + \alpha_{sc}) d)$$

Since $d = 1 \text{ cm}$ in all the measurement, therefore

$$\alpha_{sc} = -\ln\left(\frac{I}{I_{ref}}\right) - \alpha_{abs}$$

α_{abs} was calculated from absorption cross section of Si QDs ($\sigma_{abs} = 2 \times 10^{-18} \text{ cm}^2$ at 850 nm ^[1]) and the concentration of Si QDs N [cm^{-3}] in different samples. For an optical path of 1 cm this is a negligible value (only 0.007 cm^{-1} for 0.1 wt. \% loading). As a result, the scattering coefficient α_{sc} of the nanocomposites could be obtained.

Current-voltage measurement

A commercial monocrystal Si solar cell (Digi-Key, SM141K08L, $88 \times 15 \text{ mm}$) was directly coupled to one edge of the LSC by a commercial glass glue, with excess part covered by black tapes. Current–voltage characteristics were then carried out by applying an external potential bias to the device while recording the generated photocurrent with a Keithley model 2400 digital source meter. The light source was an LED lamp (SINUS-70, Wavelabs) calibrated with the light intensity to 100 mW/cm^2 at AM 1.5 G solar light condition by a certified silicon solar cell (Fraunhofer ISE).

Section S2. Characterization of Starting Materials

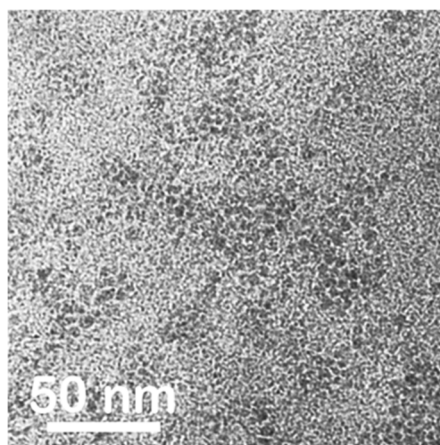


Figure S2. TEM image of the as-synthesized ester capped Si QDs, obtained from a drop-casted solution on a graphene supporting mesh.

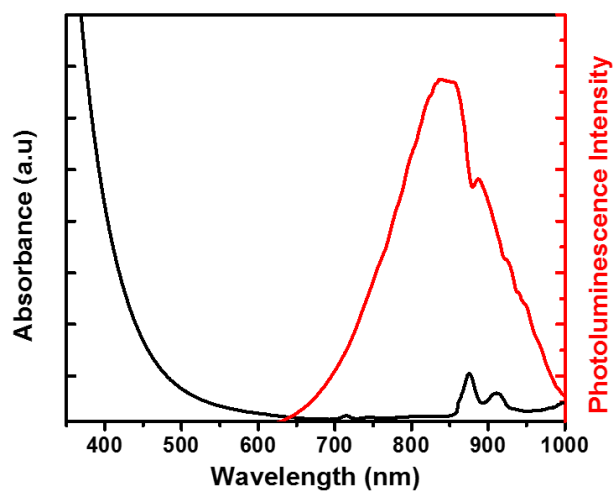


Figure S3. UV-Vis absorption (black) and fluorescence (red) spectra of Si QDs in toluene solution. Absorption at 875 nm and 910 nm are C-H overtones from toluene and capping ligand on Si QDs. The fluorescence spectrum was obtained in an integrating sphere with an excitation wavelength of 440 nm (toluene absorption dip at 875 nm can be noticed).

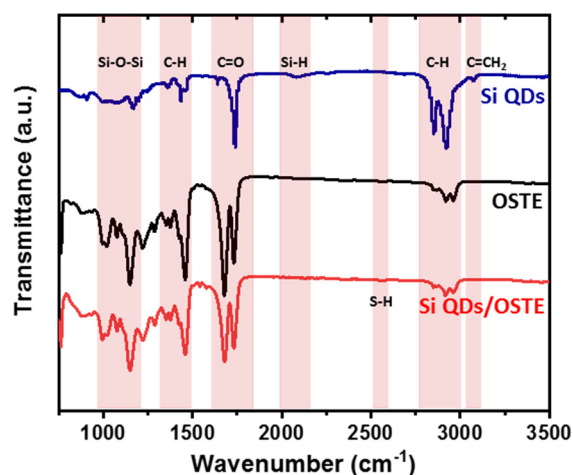


Figure S4. FTIR spectra of ester capped Si QDs, OSTE and Si QDs/OSTE samples.

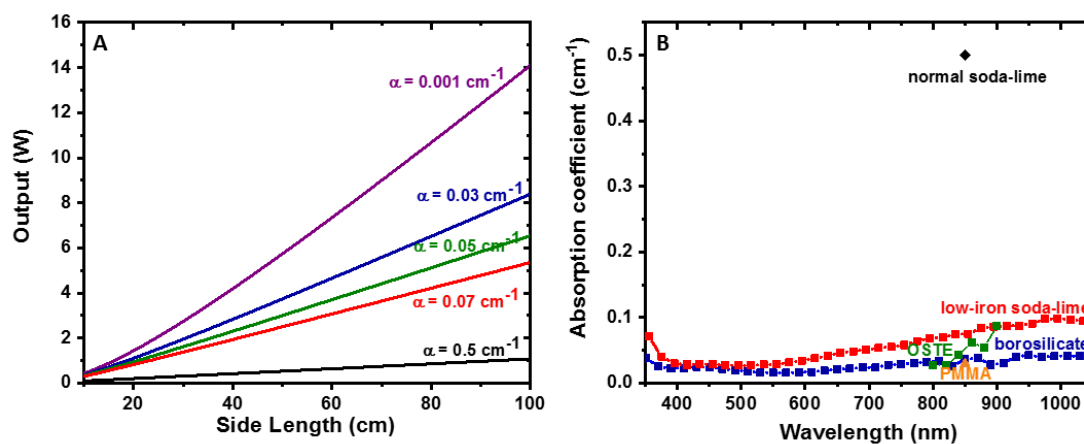


Figure S5. (A) Device optical power output calculation results based on different matrix absorption coefficients for a square shaped LSC. (B) Absorption coefficient spectral dependence of low-iron soda-lime glass, borosilicate glass and OSTE polymer which used in this work, as well as reported absorption coefficients of normal soda-lime glass and PMMA.^[2]

Section S3. Nanocomposite characterization

Table S1. Derived D values from previous work^[3] under different T/E ratio, and corresponding PLQY results measured from present work.

T/E ratio	value of D	QY ₂ in Previous work (QY ₁ =0.25)	QY ₂ in present work (QY ₁ =0.4)
1/1	0.92	0.31	0.47
1.5/1	0.85	0.37	0.48
2/1	0.73	0.45	0.56

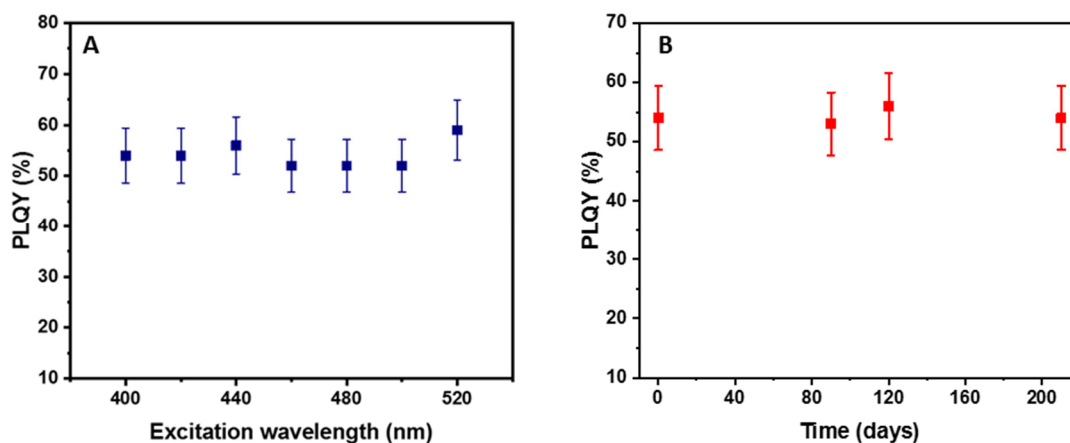


Figure S6. (A) Dependence of the PLQY on the excitation wavelength (a large error appears when the excitation wavelength is longer than 520 nm due to poor absorption in Si QDs) and (B) stability under ambient environment for the sample of Si QDs/OSTE nanocomposite with T/E ratio of 2/1 laminated in glass. For the stability investigation, the laminated sample was stored in a box without inert atmosphere protection, and taken out for PLQY measurements at different intervals.

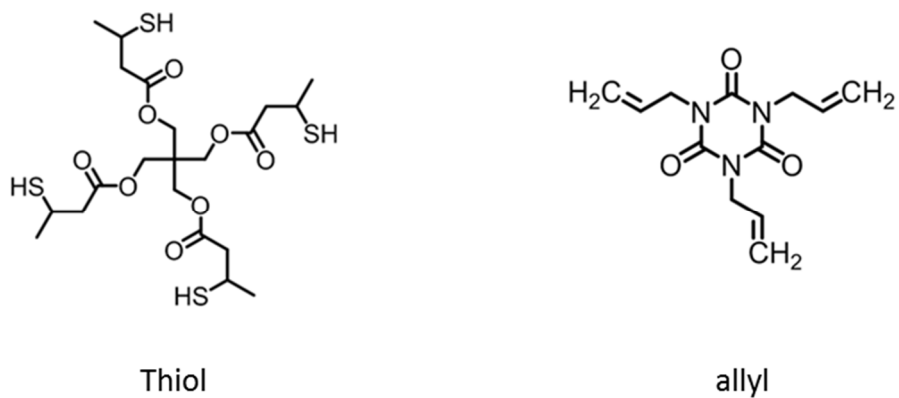


Figure S7. Molecular structures of the thiol and allyl monomers used in this work.

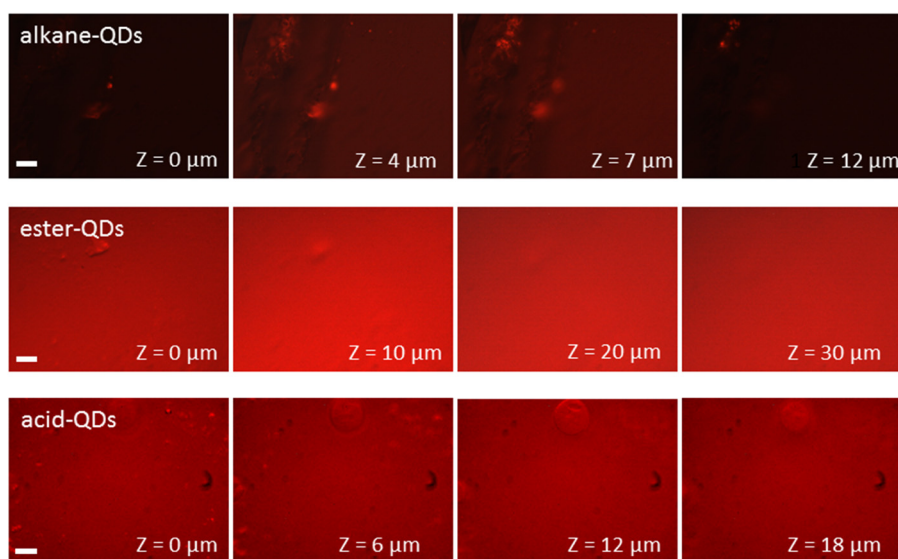


Figure S8. Real color micro-PL images at different depth Z of Si QDs/OSTE nanocomposites prepared with QDs capped by different kinds of ligand (scale bar is 10 μm). Ester ligands provide the most uniform nanoparticle distribution in the polymer.

Table S2. PLQY measured only from the top and bottom surfaces of LSCs (50 mm × 15 mm × 1 mm) and from the whole LSCs, respectively. For measuring PLQY from the top and bottom surfaces, the edges were covered by a layer of black tape and a layer of white tape, successively. The black tape was used to absorb all the emitted photons from the edges, and the white tape, which covered on the black tape, was employed to avoid additional absorption of light in the integrated sphere by the black tape. The radiation emitted to the escape cone is 25%, which is exactly the relative fraction for the emitted light in case of ester passivation. Larger values observed for alkane- and acid-QDs indicate scattering.

QDs	Loading amount of QDs	PLQY of overall device	PLQY from faces	PLQY face/PLQY overall
Alkane-QDs	0.025 wt%	43±4%	15±1%	35±5%
Ester-QDs	0.025 wt%	52±5%	13±1%	25±3%
Acid-QDs	0.025 wt%	50±5%	14±1%	28±4%

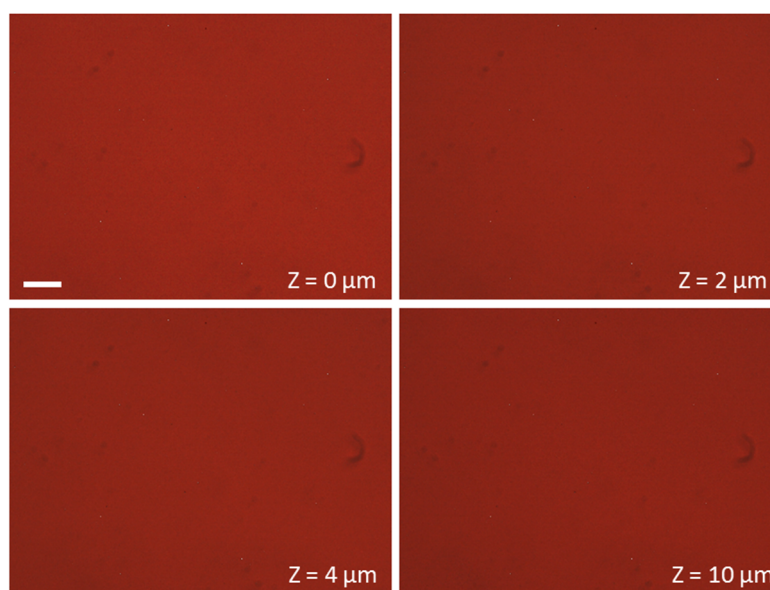


Figure S9. Real color micro-PL images taken at different depth Z of LSC fabricated with Si QDs/OSTE nanocomposite with QDs loading of 0.05 wt% (scale bar is 10 μm).

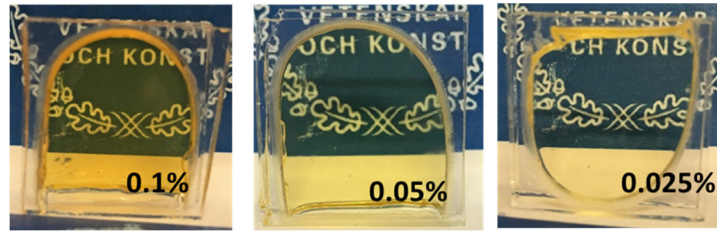


Figure S10. Photographs of small-sized LSC based on Si QDs/OSTE nanocomposite with different QDs loading (wt%)

Table S3. Parameters used in the calculations of output power for the samples with different QDs loading (wt%).

parameters	QDs loading of 0.025%	QDs loading of 0.05%	QDs loading of 0.1%	QDs loading of 0.05%-double thickness
T (at 500nm)	0.89	0.79	0.62	0.62
α_{sc}	0.036	0.091	0.288	0.091

For all the samples, PLQY is 0.55, δ is 0.75, η is 0.6, k is 1.14, α_{re} is 0.007 cm^{-1} and α is 0.04 cm^{-1} .

Negative stain effect

Since the organic ligand solution could not be removed completely from QDs solid, as we can still observe the $\nu_{\text{C}=\text{CH}_2}$ stretching mode from FTIR spectrum of Si QDs (Figure S3), the residual ligands will enter the polymer matrix together with the QDs. They are prone to form some irregular micro-droplets or nano-droplets in the matrix. In the polymer matrix, QDs prefer to stay in the ligand solution rather than the polymer matrix due to better polarity matching. Therefore, the QDs become distributed in the droplets. One should bear in mind that the atomic weight of Si QDs is low, and on the other side, there are numerous sulfur atoms in the OSTE polymer. Therefore, if the residual ligand solution is condensed in the polymer matrix, together with the heavy polymer background with sulfur atoms, there is a strong possibility that Si QDs will appear as lighter components in a bright-field TEM image.

Section S4. Theoretical Derivations

Relationship between scattering and QDs concentration

We can obtain $\alpha_{sc}(N)$ for the case of nanocrystal agglomeration from simple statistics. Consider nanoparticles randomly distributed in a volume. We stipulate that due to diffusion, difference in polarity with the monomer, etc. they tend to aggregate into clusters when within a certain interaction radius r . Let's assume that in a sphere with this radius the average number of particles is $\bar{n} = N \cdot \frac{4}{3}\pi r^3$. From Poisson statistics the cumulative distribution function to have up to k particles in this sphere is a regularized upper incomplete gamma function:

$$Q\left(k + 1, \frac{4}{3}\pi N r^3\right) = \frac{1}{k!} \int_{\frac{4}{3}\pi N r^3}^{\infty} x^k \exp(-x) dx$$

First, let our sphere of choice be centered on a test particle and the radius r to be an inter-particle distance. Then derivation of the function Q by r yields probability density function of having a distance r to the n -th neighbor. Index $n = k + 1$ because for $k = 0$ (no particles in the sphere) distance r is the distance to the first neighbor. Taking the derivative, using integral tables ^[4], immediately yields:

$$p_n(r) = \frac{3\left(\frac{4}{3}\pi N\right)^n}{(n-1)!} \cdot r^{3n-1} \cdot \exp\left(-\frac{4}{3}\pi N r^3\right)$$

which is a known expression in the information theory ^[5]. For $n = 1$ one obtains

$$p_1(r) = 4\pi N \cdot r^2 \cdot \exp\left(-\frac{4}{3}\pi N r^3\right)$$

which is a nearest neighbor distribution in 3D (Weibull distribution), first introduced in ^[6].

Instead of the inter-particle distance distribution we are more interested here in the distribution of agglomerates by the number of constituting particles. Now we can consider the sphere to be at any position inside the volume and its radius not being bound to another particle. Then from Poisson statistics the probability density function of having k particles in the sphere with a given radius r :

$$q_k = \frac{\bar{n}^k \cdot \exp(-\bar{n})}{k!}$$

A single nanocrystal has its Rayleigh scattering cross-section proportional to the particle radius R_1 as $\sigma_{sc} = \beta R_1^6$. When two particles agglomerate their volume doubles as compared to a single particle. So the cluster has then an effective radius of $R_2 = \sqrt[3]{2} R_1$ and its scattering cross-section becomes $\sigma_{sc_2} = \beta R_2^6 = 2^2 \sigma_{sc}$. For an k -particle agglomerate one can write $\sigma_{sc_k} = k^2 \sigma_{sc}$. The concentration of clusters with k particles is $N_k = N q_k / k$. Then the total linear scattering coefficient is a sum of those from each size of clusters:

$$\alpha_{sc}(N) = \sum_k \alpha_{sc,k} = \sum_k \sigma_{sc,k} N_k = \sigma_{sc} N \cdot \exp(-\bar{n}) \sum_{k=1}^{\infty} k \frac{\bar{n}^k}{k!} = \sigma_{sc} N \cdot \bar{n} = \frac{4}{3} \pi r^3 \sigma_{sc} N^2$$

So in the case of agglomeration the scattering coefficient is proportional to the square of the concentration. It is also very sensitive to the material-dependent interaction distance r , being proportional to the power of 3. Alternatively, it can be described in a simple way as a scattering coefficient for a single particle times the average number of particles in a cluster.

Effective scattering coefficient for a triplex configuration of LSC

In a triplex configuration of LSC, the nanocomposite is laminated between two sheets of optically clean glass. As shown in Figure S11, the light propagation is shortened within the nanocomposite layer in this kind of configuration, compared to only a single nanocomposite layer for an LSC.

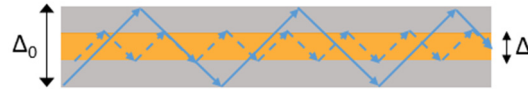


Figure S11. Illustration of light propagation in the LSC with a triplex configuration (solid arrow line), as comparing to the light propagation only in nanocomposite layer (dashed arrow line).

Due to absence of scattering in the optical glass, the effective scattering coefficient of the triplex configuration can be estimated as:

$$\alpha'_{sc} = \frac{\Delta}{\Delta_0} \alpha_{sc},$$

which is lower than the intrinsic scattering coefficient of the nanocomposite.

Section S5. Device characterization

Table S4. Photovoltaic Parameters of LSC devices ($9 \times 9 \times 0.3 \text{ cm}^3$) with and without QDs.

sample	G^a	J_{sc} (mA/cm ²)	V_{oc} (V)	FF	PCE (%)
LSC without QDs	3.21	0.141	3.67	0.611	0.317
LSC with QDs	3.21	0.500	4.37	0.675	1.47

^a G is geometric factor of the LSC device, which is defined by the ratio of the top area (A_{top}) and the edge area (A_{edge}). Since thickness of the float glass used in this work is 0.2 cm, the overall thickness of the device is 0.7 cm. Therefore, $G = \frac{A_{top}}{A_{edge}} = \frac{9 \times 9}{9 \times 0.7 \times 4} = 3.21$.

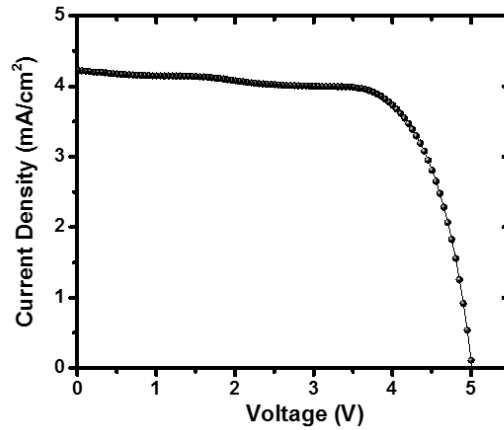


Figure S12. J - V curve of the custom-sized Si solar cell (active area of $9 \times 0.7 \text{ cm}^2$) illuminated by solar simulator directly, with J_{sc} of 4.22 mA/cm^2 , V_{oc} of 5.01 V , FF of 0.706 and PCE of 14.93% .

The optical power conversion efficiency of the LSC with QDs ($9 \times 9 \times 0.3 \text{ cm}^3$) could be calculated as^[7]

$$\eta_{opt} = \frac{P_{out}}{P_{in}} = \frac{J_{LSC}}{J_{Si} \times G} = \frac{0.5}{4.22 \times 3.21} = 3.7\%.$$



Figure S13. Photograph of LSC based on Si QDs/OSTE nanocomposite (QDs loading of 0.05 wt%) with different thickness: left-3 mm and right-6 mm. Inserted image shows edges of the two triplex devices.

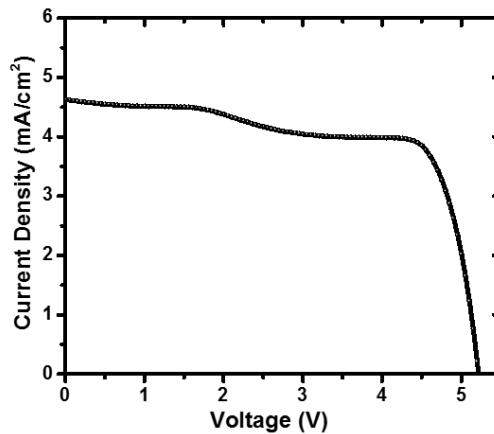


Figure S14. J - V curve of the Si solar cell (active area of $9 \times 1 \text{ cm}^2$) illuminated by solar simulator directly.

Table S5. Photovoltaic Parameters of silicon solar cells directly illuminated by solar simulator and attached on LSC device with Si QDs ($9 \times 9 \times 0.6 \text{ cm}^3$).

sample	J_{sc} (mA/cm ²)	V_{oc} (V)	FF	PCE (%)
Si solar cell	4.63	5.22	0.719	17.4
LSC with QDs	0.82	4.74	0.706	2.74

The optical power conversion efficiency of the LSC with QDs ($9 \times 9 \times 0.6 \text{ cm}^3$) could be calculate as

$$\eta'_{opt} = \frac{P_{out}}{P_{in}} = \frac{J_{LSC}}{J_{Si} \times G} = \frac{0.82}{4.63 \times 2.25} = 7.9\%.$$

Reference

- [1] J. Valenta, M. Greben, Z. Remeš, S. Gutsch, D. Hiller, M. Zacharias, *Appl. Phys. Lett.* **2016**, *108*, 023102.
- [2] F. Meinardi, F. Bruni, S. Brovelli, *Nat. Rev. Mater.* **2017**, *2*, 17072.
- [3] A. Marinins, R. Zandi Shafagh, W. van der Wijngaart, T. Haraldsson, J. Linnros, J. G. C. Veinot, S. Popov, I. Sychugov, *ACS Appl. Mater. Interfaces* **2017**, *9*, 30267-30272.
- [4] I. S. Gradshteyn, I. M. Ryzhik, *Table of Integrals, Series and Products*. Elsevier: US, 2015; Vol. 8th edition.
- [5] M. Haenggi, *IEEE Trans. Inf Theory* **2005**, *51*, 3584-3586.
- [6] P. Hertz, *Math. Ann.* **1909**, *67*, 387.
- [7] a) Y. Zhou, H. Zhao, D. Ma, F. Rosei, *Chem. Soc. Rev.* **2018**, *47*, 5866-5890; b) F. Purcell-Milton, Y. K. Gun'ko, *J. Mater. Chem.* **2012**, *22*, 16687-16697.